TÜBİTAK

Turkish Journal of Physics

http://journals.tubitak.gov.tr/physics/

Research Article

Turk J Phys
(2022) 46: 252 – 275

doi:10.55730/1300-0101.2731

Dynamic multicritical phase diagrams of the mixed spin (2, 5/2) Blume-Emery-Griffiths model with repulsive biquadratic coupling

Mustafa GENÇASLAN, **Mustafa KESKİN***
Department of Physics, Faculty of Science, Erciyes University, Kayseri, Turkey

Received: 17.11.2022 • **Accepted/Published Online:** 30.11.2022 • **Final Version:** 27.12.2022

Abstract: We investigated the dynamic phase transitions (DPTs) in the mixed spin (2, 5/2) Blume-Emery-Griffiths model with repulsive biquadratic interaction in the presence of a time-varying magnetic field. We used the path probability method to obtain the set of the dynamic equations. We numerically solved these dynamic equations to characterize the nature of first- and second-order phase transitions and to find the DPT temperatures as well as obtain the phases in the system. We constructed the dynamic phase diagrams (DPDs) in reduced temperature and amplitude of oscillating magnetic field plane. We observed that the DPDs display richer, complex and more topological various type of phase diagrams. In particular, DPDs exhibit the disordered phase, antiquadrupolar or staggered phase, six different ferrimagnetic phases, three different nonmagnetic phases, and numerous mixed phases. DPDs also display two dynamic tricritical points for only smaller values of crystal-field interactions, multiple critical end and double critical end points, one zero-temperature critical point, one inverse critical end point, and a quadruple point depending on interaction parameters. The system always shows the reentrant behaviors for the higher values of magnetic field amplitude, but it does not exhibit the dynamic tricritical behavior for higher values of crystal-field parameter.

Keywords: Mixed spin (2, 5/2) Ising model, path probability method, dynamic phase transition, dynamic phase diagram, reentrant behavior, special critical points

1. Introduction

The mixed spin-2 and spin-5/2 Blume-Emery-Griffiths (BEG) model is the most general mixed spin-2 and spin-5/2 Ising model with Hamiltonian composed of bilinear, biquadratic nearest-neighbor pair interactions and crystal-field term or a single-ion anisotropy. Although the mixed spin-2 and spin-5/2 Ising system is the complex and more difficult to work on, the system is the most used and the most studied system among the mixed Ising systems. Two important reasons are follows: (1) The system gives very rich phase diagrams and interesting critical behaviors. (2) It is one of the suitable prototypical systems to examine many molecular-based magnetic materials, such as N(n-C_4H_9)$_4$$Fe^{II}Fe^{III}$($C_2O_4$)$_3$ [1], A$Fe^{II}Fe^{III}$(C_2O_4)$_3$ [A = N(n-C_nH_{2n+1})$_4$, n = 3–5] [2–6], and A$M^{II}Fe^{III}$(C_2O_4)$_3$ (A = N(n-C_3H_7)$_4$ M=Mn, Fe) [2, 7] as well as the other compounds, for instance Fe_7S_8 [8], $BiFeO_3$/$YMnO_3$ bilayer films, Mn substituted polycrystalline $ErFeO_3$ [9], the diluted $Fe^{II}Fe^{III}$ bimetallic oxalates [10]. On the other hand, in spite of the mixed spin (2, 5/2) Ising system

*Correspondence: keskin@erciyes.edu.tr

with the simple Hamiltonian has been the most used system, the mixed spin (2, 5/2) BEG model has not been used much and not been studied extensively. The reason is that Hamiltonian of this system contains the biquadratic nearest-neighbor pair interaction that makes it difficult to work on the system. At the same time, the repulsive biquadratic coupling provides very rich phase diagrams and interesting critical behaviors in all Ising systems. For example, the BEG model in pure Ising systems, such as the spin-1 BEG [11–18] and spin-3/2 BEG model [19–22], and the mixed spin (1, 3/2) Ising system [23] exhibit very rich equilibrium phase diagrams [11–17, 19–21] and dynamic phase diagrams [18, 22, 23]. An early attempt to investigate the mixed spin (2, 5/2) BEG model was made by Albayrak [24] who studied the system on the Bethe lattice by utilizing the exact recursion equations. He presented the equilibrium phase diagrams in two different planes and found that the system exhibits very rich critical behaviors, such as the tricritical and critical end points, compensation temperatures, etc. Dynamic magnetic behaviors of the mixed spin (2, 5/2) BEG model were examined Ertaş et al. [25] by employing the mean-field approach based on Glauber-type stochastic dynamics that has been also called the dynamic mean-field approximation (DMFA). In particular, they characterized the nature (first- or second-order phase transitions) of dynamic phase transitions (DPT) and obtained DPT temperatures and presented the dynamic phase diagram (DPDs). They found that DPDs display a novel multicritical topology, such as the disordered, antiquadrupolar and three distinct ferrimagnetic, fundamental phases as well as ten different mixed phases. Moreover, the DPDs also exhibit the dynamic tricritical point, dynamic double critical end points, triple and quadruple special critical points.

The purpose of the present work is to investigate the dynamical aspect of the mixed spin (2, 5/2) BEG model within the path probability method [26]. In particular, we investigated the DPTs in the model and presented the DPDs in the reduced temperature and the amplitude of oscillating magnetic field plane. The reason we utilized the path probability method (PPM) is that it provides following advantages over the DMFA. (1) PPM supplies three rate constants in the model, whereas the DMFA provides only one rate constant. (2) PPM provides more couplings among the order parameters. (3) Formulations of the dynamic equations are simpler and systematic than the DMFA. Moreover, the PPM has been successfully utilized to examine the dynamic features of many different physical systems and describing various physical phenomena (see [27–33] and references therein). The organization of the remaining part of the paper is as follows: In Section 2, the model and its formulation, namely the derivation of the set of the average dynamic equations for the order parameters, are given. Section 3 contains the numerical results and discussion. Finally, summary and concussion are given in Section 4.

2. Model and formulation

The mixed spin (2, 5/2) BEG model is a mixed spin (2, 5/2) Ising model Hamiltonian with bilinear (J) and biquadratic (K) nearest-neighbor pair interactions in which a single-ion anisotropy parameter or crystal-field interaction (D) is included. The Hamiltonian of the mixed spin (2, 5/2) BEG model on a two interpenetrating square sublattices in a presence of a time-dependent oscillating external magnetic field is

$$\mathcal{H} = -J \sum_{<ij>} \sigma_i^A S_j^B - K \sum_{<ij>} (\sigma_i^A)^2 (S_j^B)^2 - D \left[\sum_i (\sigma_i^A)^2 + \sum_j (S_j^A)^2 \right] - H \left(\sum_i \sigma_i^A + \sum_j S_j^B \right), \quad (2.1)$$

where $\sigma_i^A = \pm 2, 0, \pm 1$ values, and $S_j^B = \pm 5/2, \pm 3/2, \pm 1/2$ on sites of the sublattices A and B, respectively. H is a time-dependent oscillating external magnetic field and given by

$$H = H_0 \, cos(\omega \, t), \tag{2.2}$$

where H_0 and $\omega = 2\pi\nu$ are the amplitude and the angular frequency of the oscillating field, respectively. The average value of each of the spin states, also called as state, point or internal variables, are indicated by X_1^A, X_2^A, X_3^A, X_4^A, X_5^A that the fraction of spin takes $+2, +1, 0, -1, -2$ values, respectively, on the sites of A sublattice and X_1^B, X_2^B, X_3^B, X_4^B, X_5^B, X_6^B with values $+\frac{5}{2}, +\frac{3}{2}, +\frac{1}{2}, -\frac{5}{2}, -\frac{3}{2}, -\frac{1}{2}$ on the B sublattice. X_i^A and X_j^B obey the following normalization relations:

$$\sum_{i=1}^{5} X_i^A = 1, \tag{2.3}$$

and

$$\sum_{j=1}^{6} X_j^B = 1. \tag{2.4}$$

The model contains following four order parameters for the sublattice A: (1) The average magnetization or dipole moment, $m^A \equiv < \sigma_i^A >$, (2) the quadrupole moment, $q^A \equiv < (\sigma_i^A)^2 >$, (3) the octupole moment, $r^A \equiv < (\sigma_i^A)^3 >$, (4) the hexadecapole moment, $o^A \equiv < (\sigma_i^A)^4 >$. On the other hand, the model also contains the following five order parameters for B sublattice: (1) The average magnetization or dipole moment, $m^B \equiv < S_j^B >$, (2) the quadrupole moment, $q^B \equiv < (S_j^B)^2 >$, (3) the octupole moment, $r^B \equiv < (S_j^B)^3 >$, (4) the hexadecapole moment, $o^B \equiv < (S_j^B)^4 >$ and (5) the dotriacontapole moment, $p^B \equiv < (S_j^B)^5 >$. The average order parameters for the sublattices A and B are written in terms of the point variables (X_i^A and X_j^B) and are given by,

$$\begin{aligned} m^A &= 2X_1^A + X_2^A - X_4^A - 2X_5^A, \\ q^A &= 4X_1^A + X_2^A + X_4^A + 4X_5^A, \\ r^A &= 8X_1^A + X_2^A - X_4^A - 8X_5^A, \\ o^A &= 16X_1^A + X_2^A + X_4^A + 16X_5^A, \end{aligned} \tag{2.5}$$

and

$$\begin{aligned} m^B &= \frac{5}{2}X_1^B + \frac{3}{2}X_2^B + \frac{1}{2}X_3^B - \frac{1}{2}X_4^B - \frac{3}{2}X_5^B - \frac{5}{2}X_6^B, \\ q^B &= \frac{25}{4}X_1^B + \frac{9}{4}X_2^B + \frac{1}{4}X_3^B + \frac{1}{4}X_4^B + \frac{9}{4}X_5^B + \frac{25}{4}X_6^B, \\ r^B &= \frac{125}{8}X_1^B + \frac{27}{8}X_2^B + \frac{1}{8}X_3^B - \frac{1}{8}X_4^B - \frac{27}{8}X_5^B - \frac{125}{8}X_6^B, \\ o^B &= \frac{625}{16}X_1^B + \frac{81}{16}X_2^B + \frac{1}{16}X_3^B + \frac{1}{16}X_4^B + \frac{81}{16}X_5^B + \frac{625}{16}X_6^B, \\ p^B &= \frac{3125}{32}X_1^B + \frac{243}{32}X_2^B + \frac{1}{32}X_3^B - \frac{1}{32}X_4^B - \frac{243}{32}X_5^B - \frac{3125}{32}X_6^B. \end{aligned} \tag{2.6}$$

X_i^A can also be written in terms of m^A, q^A, r^A, o^A by using Eqs. (2.3) and (2.5) for the sublattice A,

$$\begin{aligned}
X_1^A &= -\frac{1}{12}m^A + \frac{1}{12}r^A - \frac{1}{24}q^A + \frac{1}{24}o^A,\\
X_2^A &= \frac{2}{3}m^A + \frac{2}{3}q^A - \frac{1}{6}r^A - \frac{1}{6}o^A,\\
X_3^A &= 1 - \frac{5}{4}q^A + \frac{1}{4}o^A,\\
X_4^A &= -\frac{2}{3}m^A + \frac{2}{3}q^A + \frac{1}{6}r^A - \frac{1}{6}o^A,\\
X_5^A &= \frac{1}{12}m^A - \frac{1}{24}q^A - \frac{1}{12}r^A + \frac{1}{24}o^A.
\end{aligned} \tag{2.7}$$

Similarly, X_j^B is obtained in terms of linear combinations of the order parameters by utilizing Eqs. (2.4) and (2.6) for the B sublattice as

$$\begin{aligned}
X_1^B &= \frac{3}{640}m^B - \frac{5}{96}q^B - \frac{1}{48}r^B + \frac{1}{48}o^B + \frac{1}{120}p^B + \frac{3}{256},\\
X_2^B &= -\frac{25}{384}m^B + \frac{13}{32}q^B + \frac{13}{48}r^B - \frac{1}{16}o^B - \frac{1}{24}p^B - \frac{25}{256},\\
X_3^B &= \frac{75}{64}m^B - \frac{17}{48}q^B - \frac{17}{24}r^B + \frac{1}{24}o^B + \frac{1}{12}p^B + \frac{75}{128},\\
X_4^B &= -\frac{75}{64}m^B - \frac{17}{48}q^B + \frac{17}{24}r^B + \frac{1}{24}o^B - \frac{1}{12}p^B + \frac{75}{128},\\
X_5^B &= \frac{25}{384}m^B + \frac{13}{32}q^B - \frac{13}{48}r^B - \frac{1}{16}o^B + \frac{1}{24}p^B - \frac{25}{256},\\
X_6^B &= -\frac{3}{640}m^B - \frac{5}{96}q^B + \frac{1}{48}r^B + \frac{1}{48}o^B - \frac{1}{120}p^B + \frac{3}{256}.
\end{aligned} \tag{2.8}$$

Now, we can apply the PPM [26] to find the average dynamic order parameters for the sublattices A and B. In the PPM, the rate of change of the state variables is defined as

$$\frac{dX_i}{dt} = \sum_{i\neq j}(\chi_{ji} - \chi_{ij}). \tag{2.9}$$

χ_{ij} indicates the path probability rate for the system to run from state i to j. The detailed balancing requires that

$$\chi_{ji} \neq \chi_{ij} \tag{2.10}$$

Kikuchi [26] introduced two equations or recipes for χ_{ij}. We used Kikuchi's recipe or equation II as

$$\chi_{ij} = k_{ij}\, Z^{-1} exp\left[\left(-\frac{\beta}{N}\right)\frac{\partial E}{\partial X_j}\right] X_i, \tag{2.11}$$

where $\beta = 1/k_BT$, k_B is the Boltzmann constant and fixed as $k_B = 1.0$ in all the numerical calculations and k_{ij} are rate constants with $k_{ij} = k_{ji}$. The system contains the following three rate constants: (1) $k_{12} = k_{34} = k_1$ expresses the insertion or removal of spin particles through the lattices which relates the translation of spin particles, (2) $k_{14} = k_{23} = k_2$ is associated the rotation of spin particles on a given site. (3) $k_{13} = k_{24} = k_3$ is associated with the simultaneous translation and rotation of particles; hence k_3 can be written in terms of k_1 and k_2 as $k_3 = \sqrt{k_1 k_2}$. We considered that the insertion, removal or rotation of two spin particles do not occur simultaneously, that is, only a single jump takes place. The existence of rate constants is illustrated in Table 1. N represents the number of spin particles or lattice sites and Z is the partition function and is written as

$$\begin{aligned} Z^A &= \sum_{i=1}^{5} exp\Big[-\frac{\beta}{N}\Big(\frac{\partial E}{\partial X_i^A}\Big)\Big], \\ Z^B &= \sum_{j=1}^{6} exp\Big[-\frac{\beta}{N}\Big(\frac{\partial E}{\partial X_j^B}\Big)\Big], \end{aligned} \tag{2.12}$$

where Z^A and Z^B represent the partition functions for A and B sublattices, respectively. E is the internal energy per site that can be expressed a function of the X_i^A and X_j^B by utilizing Eqs. (2.1), (2.5) and (2.6) as

$$\begin{aligned} \frac{E}{N} =& -J(2X_1^A + X_2^A - X_4^A - 2X_5^A)(\frac{5}{2}X_1^B + \frac{3}{2}X_2^B + \frac{1}{2}X_3^B - \frac{1}{2}X_4^B - \frac{3}{2}X_5^B - \frac{5}{2}X_6^B) \\ & - K(4X_1^A + X_2^A + X_4^A + 4X_5^A)(\frac{25}{4}X_1^B + \frac{9}{4}X_2^B + \frac{1}{4}X_3^B + \frac{1}{4}X_4^B + \frac{9}{4}X_5^B + \frac{25}{4}X_6^B) \\ & - D(4X_1^A + X_2^A + X_4^A + 4X_5^A + \frac{25}{4}X_1^B + \frac{9}{4}X_2^B + \frac{1}{4}X_3^B + \frac{1}{4}X_4^B + \frac{9}{4}X_5^B + \frac{25}{4}X_6^B) \\ & - H(2X_1^A + X_2^A - X_4^A - 2X_5^A+) - H(\frac{5}{2}X_1^B + \frac{3}{2}X_2^B + \frac{1}{2}X_3^B - \frac{1}{2}X_4^B - \frac{3}{2}X_5^B - \frac{5}{2}X_6^B). \end{aligned} \tag{2.13}$$

Now, the set of coupling average dynamic equations for order parameters can be obtained by using Eqs. (2.7)-(2.13) as

$$\begin{aligned} &\Omega\frac{dm^A}{d\xi} = \\ &\Big\{\Big[\frac{1}{12}(k_2 - k_1)\sinh(a_1) + \frac{2}{3}(k_2 - k_1)\sinh(2a_1) + \frac{1}{4}(2k_3 - 11k_2 + k_1)\cosh(a_1) \\ &+ 2(k_1 - 2k_3)\cosh(2a_1) - k_1\Big]m^A \\ &+ \Big[\frac{1}{8}(-2k_3 + 21k_2 - 19k_1)\sinh(a_1) + (4k_3 - k_2 - 3k_1)\sinh(a_1) + \frac{1}{24}(k_2 - k_1)\cosh(a_1) \\ &+ \frac{2}{3}(k_2 - k_1)\cosh(2a_1)\Big]q^A \end{aligned} \tag{2.14}$$

$$+\left[\frac{1}{6}(k_2-k_1)\sinh(2a_1)-\frac{1}{4}(2k_3-3k_2+k_1)\cosh(a_1)+\frac{1}{2}(2k_3-k_2-k_1)\cosh(2a_1)\right]r^A$$
$$+\left[\frac{1}{8}(2k_3-5k_2+3k_1)\sinh(a_1)-\frac{1}{2}(2k_3-k_2-k_1)\sinh(2a_1)-\frac{1}{24}(k_2-k_1)\cosh(a_1)\right.$$
$$\left.-\frac{1}{6}(k_2-k_1)\cosh(2a_1)]o^A\right.$$
$$\left.+2k_1\sinh(a_1)+4k_1\sinh(2a_1)\right\}/k\left[2\cosh(a_1)e^{b_1}+2\cosh(2a_1)e^{4b_1}+1\right]$$

$$\Omega\frac{dq^A}{d\xi}=$$
$$\left\{\left[\frac{1}{12}(k_2-k_1)\cosh(a_1)+\frac{2}{3}(k_2-k_1)\cosh(2a_1)-\frac{1}{12}(6k_3+k_2-k_1)\sinh(a_1)\right.\right.$$
$$\left.-\frac{2}{3}(6k_3-k_2+7k_1)\sinh(2a_1)\right]m^A$$
$$+\left[\frac{1}{24}(k_2-k_1)\sinh(a_1)+\frac{2}{3}(k_2-k_1)\sinh(2a_1)+\frac{1}{24}(6k_3-k_2-53k_1)\cosh(a_1)\right.$$
$$\left.+\frac{2}{3}(6k_3-k_2-8k_1)\cosh(2a_1)-k_1\right]q^A \qquad (2.14)$$
$$+\left[\frac{1}{12}(k_1-k_2)\cosh(a_1)+\frac{1}{6}(k_1-k_2)\cosh(2a_1)+\frac{1}{12}(6k_3+k_2-7k_1)\sinh(a_1)\right.$$
$$\left.+\frac{1}{6}(6k_3+k_2-7k_1)\sinh(2a_1)\right]r^A$$
$$+\left[\frac{1}{24}(k_1-k_2)\sinh(a_1)+\frac{1}{6}(k_1-k_2)\sinh(2a_1)-\frac{1}{24}(6k_3-k_2-5k_1)\cosh(a_1)\right.$$
$$\left.-\frac{1}{6}(6k_3-k_2-5k_1)\cosh(2a_1)\right]o^A$$
$$\left.+2k_1\cosh(a_1)+8k_1\cosh(2a_1)\right\}/k\left[2\cosh(a_1)e^{b_1}+2\cosh(2a_1)e^{4b_1}+1\right]$$

$$\Omega\frac{dr^A}{d\xi}=$$
$$\left\{\left[\frac{1}{12}(k_2-k_1)\sinh(a_1)+\frac{2}{3}(k_2-k_1)\sinh(2a_1)+\frac{1}{4}(6k_3-11k_2+5k_1)\cosh(a_1)\right.\right.$$
$$\left.-2(6k_3-k_2-5k_1\cosh(2a_1)\right]m^A$$
$$+\left[\frac{1}{24}(k_2-k_1)\cosh(a_1)+\frac{2}{3}(k_2-k_1)\cosh(2a_1)-\frac{1}{8}(6k_3-21k_2+15k_1)\sinh(a_1)\right.$$
$$\left.+2(6k_3-k_2-5k_1)\sinh(2a_1)\right]q^A \qquad (2.15)$$

$$+\left[\frac{1}{12}(k_1-k_2)\sinh(a_1)+\frac{1}{6}(k_1-k_2)\sinh(2a_1)-\frac{1}{4}(6k_3+3k_2-5k_1)\cosh(a_1)\right.$$
$$\left.+\frac{1}{2}(6k_3-5k_2-5k_1)\cos(2a_1)-k_1\right]r^A$$
$$+\left[\frac{1}{24}(k_1-k_2)\cosh(a_1)+\frac{1}{6}(k_1-k_2)\cosh(2a_1)+\frac{1}{8}(6k_3-5k_2-5k_1)\sinh(a_1)\right.$$
$$\left.-\frac{3}{2}(6k_3-k_2-k_1)\sinh(2a_1)\right]o^A$$
$$\left.+2k_1\sinh(a_1)+16k_1\sinh(2a_1)\right\}/k[2\cosh(a_1)e^{b_1}+2\cosh(2a_1)e^{4b_1}+1]$$

$$\Omega\frac{do^A}{d\xi}=$$
$$\left\{\left[\frac{1}{12}(k_2-k_1)\cosh(a_1)+\frac{2}{3}(k_2-k_1)\cosh(2a_1)-\frac{1}{12}(6k_3+k_2-31k_1)\sinh(a_1)\right.\right.$$
$$\left.-\frac{2}{3}(30k_3+k_2-31k_1)\sinh(2a_1)\right]m^A$$
$$+\left[\frac{1}{24}(k_2-k_1)\sinh(a_1)+\frac{2}{3}(k_2-k_1)\sinh(2a_1)+\frac{1}{24}(30k_3-k_2-29k_1)\cosh(a_1)\right.$$
$$\left.+\frac{2}{3}(30k_3-k_2-29k_1)\cosh(2a_1)\right]q^A \qquad (2.16)$$
$$+\left[\frac{1}{12}(k_1-k_2)\cosh(a_1)+\frac{1}{6}(k_1-k_2)\cosh(2a_1)+\frac{1}{12}(30k_3+k_2-31k_1)\sinh(a_1)\right.$$
$$\left.+\frac{1}{6}(30k_3+k_2-31k_1)\sinh(2a_1)\right]r^A$$
$$+\left[\frac{1}{24}(k_1-k_2)\sinh(a_1)+\frac{1}{6}(k_1-k_2)\sinh(2a_1)-\frac{1}{24}(30k_3-k_2+19k_1)\cosh(a_1)\right.$$
$$\left.-\frac{1}{6}(30k_3-k_2-17k_1)\cosh(2a_1)-k_1\right]o^A$$
$$\left.+2k_1\cosh(a_1)+32k_1\cosh(2a_1)\right\}/k\left[2\cosh(a_1)e^{b_1}+2cosh(2a_1)e^{4b_1}+1\right]$$

and

$$\Omega\frac{dm^B}{d\xi}=$$
$$\left\{\left[(\frac{223}{960}k_3-\frac{75}{32}k_2+\frac{107}{960}k_1)\cosh\left(\frac{a_2}{2}\right)+(-\frac{189}{40}k_3+\frac{25}{64}k_2+\frac{747}{320}k_1)\cosh\left(\frac{3a_2}{2}\right)\right.\right.$$
$$\left.+(-\frac{625}{96}k_3-\frac{3}{64}k_2+\frac{875}{192}k_1)\cosh\left(\frac{5a_2}{2}\right)\right]m^B$$

$$
\begin{aligned}
&+\Big[(\frac{21}{16}k_3-\frac{17}{24}k_2-\frac{29}{48}k_1)\sinh\Big(\frac{a_2}{2}\Big)+(-\frac{11}{6}k_3+\frac{39}{16}k_2-\frac{29}{48}k_1)\sinh\Big(\frac{3a_2}{2}\Big)\\
&+(\frac{9}{8}k_3-\frac{25}{48}k_2-\frac{29}{48}k_1)\sinh\Big(\frac{5a_2}{2}\Big)\Big]q^B\\
&+\Big[(-\frac{23}{24}k_3+\frac{17}{12}k_2-\frac{11}{24}k_1)\cosh\Big(\frac{a_2}{2}\Big)+(3k_3-\frac{13}{8}k_2-\frac{11}{8}k_1)\cosh\Big(\frac{3a_2}{2}\Big)\\
&+(\frac{25}{12}k_3+\frac{5}{24}k_2-\frac{55}{24}k_1)\cosh\Big(\frac{5a_2}{2}\Big)\Big]r^B\\
&+\Big[(-\frac{1}{8}k_3+\frac{1}{12}k_2+\frac{1}{24}k_1)\sinh\Big(\frac{a_2}{2}\Big)+(\frac{1}{3}k_3-\frac{3}{8}k_2+\frac{1}{24}k_1)\sinh\Big(\frac{3a_2}{2}\Big)\\
&+(-\frac{1}{4}k_3+\frac{5}{24}k_2+\frac{1}{24}k_1)\sinh\Big(\frac{5a_2}{2}\Big)\Big]o^B\\
&+\Big[(\frac{7}{60}k_3-\frac{1}{6}k_2+\frac{1}{20}k_1)\cosh\Big(\frac{a_2}{2}\Big)+(-\frac{2}{5}k_3+\frac{1}{4}k_2+\frac{3}{20}k_1)\cosh\Big(\frac{3a_2}{2}\Big)\\
&+(-\frac{1}{6}k_3-\frac{1}{12}k_2+\frac{1}{4}k_1)\cosh\Big(\frac{5a}{2}\Big)\Big]p^B\\
&+(-\frac{41}{128}k_3+\frac{75}{64}k_2+\frac{19}{128}k_1)\sinh\Big(\frac{a_2}{2}\Big)+(\frac{39}{16}k_3-\frac{75}{128}k_2+\frac{147}{128}k_1)\sinh\Big(\frac{3a_2}{2}\Big)\\
&+(\frac{175}{64}k_3+\frac{15}{128}k_2+\frac{275}{128}k_1)\sinh\Big(\frac{5a_2}{2}\Big)\Big\}\\
&/k\Big[2\cosh\Big(\frac{a_2}{2}\Big)e^{\frac{b_2}{4}}+2\cosh\Big(\frac{3a_2}{2}\Big)e^{\frac{9b_2}{4}}\Big]
\end{aligned}
\tag{2.17}
$$

$$
\begin{aligned}
&\Omega\frac{dq^B}{d\xi}=\\
&\Big\{\Big[(-\frac{49}{240}k_3+\frac{49}{240}k_1)\sinh\Big(\frac{a_2}{2}\Big)+(-\frac{93}{20}k_3+\frac{93}{20}k_1)\sinh\Big(\frac{3a_2}{2}\Big)\\
&+(-\frac{325}{24}k_3+\frac{325}{24}k_1)\sinh\Big(\frac{5a_2}{2}\Big)\Big]m^B\\
&+\Big[(-k_3-k_1)\cosh\Big(\frac{a_2}{2}\Big)+(-k_3-k_1)\cosh\Big(\frac{3a_2}{2}\Big)+(-k_3-k_1)\cosh\Big(\frac{5a_2}{2}\Big)\Big]q^B\\
&+\Big[\frac{5}{6}(k_3-k_1)\sinh\Big(\frac{a_2}{2}\Big)+\frac{8}{3}(k_3-k_1)\sinh\Big(\frac{3a_2}{2}\Big)+\frac{19}{3}(k_3-k_1)\sinh\Big(\frac{5a_2}{2}\Big)\Big]r^B\\
&+\Big[-\frac{1}{15}(k_3-k_1)\sinh\Big(\frac{a_2}{2}\Big)-\frac{4}{15}(k_3-k_1)\sinh\Big(\frac{3a_2}{2}\Big)-\frac{2}{3}(k_3-k_1)\sinh\Big(\frac{5a_2}{2}\Big)\Big]p^B\\
&+\Big[(k_3+k_1)\cosh\Big(\frac{a_2}{2}\Big)+\frac{9}{4}(k_3+k_1)\cosh\Big(\frac{3a_2}{2}\Big)+\frac{25}{4}(k_3+k_1)\cosh\Big(\frac{5a_2}{2}\Big)\Big]\Big\}
\end{aligned}
\tag{2.18}
$$

$$/k\left[2\cosh\left(\frac{a_2}{2}\right)e^{\frac{b_2}{4}}+2\cosh\left(\frac{3a_2}{2}\right)e^{\frac{9b_2}{4}}\right]$$

$$\Omega\frac{dr^B}{d\xi}=$$
$$\left\{\left[(\frac{1183}{3840}k_3-\frac{75}{128}k_2+\frac{1067}{3840}k_1)\cosh\left(\frac{a_2}{2}\right)+(-\frac{1341}{160}k_3+\frac{225}{256}k_2+\frac{9603}{1280}k_1)\cosh\left(\frac{3a_2}{2}\right)\right.\right.$$
$$\left.+(-\frac{13225}{384}k_3-\frac{75}{256}k_2+\frac{26675}{768}k_1)\cosh\left(\frac{5a_2}{2}\right)\right]m^B$$
$$+\left[(\frac{77}{64}k_3-\frac{17}{96}k_2-\frac{197}{192}k_1)\sinh\left(\frac{a_2}{2}\right)+(-\frac{107}{24}k_3+\frac{351}{64}k_2-\frac{197}{192}k_1)\sinh\left(\frac{3a_2}{2}\right)\right.$$
$$\left.+(\frac{137}{32}k_3-\frac{625}{192}k_2-\frac{197}{192}k_1)\sinh\left(\frac{5a_2}{2}\right)\right]q^B$$
$$+\left[(-\frac{119}{96}k_3+\frac{17}{48}k_2-\frac{107}{96}k_1)\cosh\left(\frac{a_2}{2}\right)+(\frac{23}{4}k_3-\frac{117}{32}k_2-\frac{131}{32}k_1)\cosh\left(\frac{3a_2}{2}\right)\right.$$
$$\left.+(\frac{577}{48}k_3+\frac{125}{96}k_2-\frac{1471}{96}k_1)\cosh\left(\frac{5a_2}{2}\right)\right]r^B$$
$$+\left[(\frac{7}{32}k_3+\frac{1}{48}k_2-\frac{23}{96}k_1)\sinh\left(\frac{a_2}{2}\right)+(\frac{13}{12}k_3-\frac{27}{32}k_2-\frac{23}{96}k_1)\sinh\left(\frac{3a_2}{2}\right)\right. \tag{2.19}$$
$$\left.+(-\frac{17}{16}k_3+\frac{125}{96}k_2-\frac{23}{96}k_1)\sinh\left(\frac{5a_2}{2}\right)\right]o^B$$
$$+\left[(\frac{7}{240}k_3-\frac{1}{24}k_2+\frac{1}{80}k_1)\cosh\left(\frac{a_2}{2}\right)+(-\frac{9}{10}k_3+\frac{9}{16}k_2+\frac{27}{80}k_1)\cosh\left(\frac{3a_2}{2}\right)\right.$$
$$\left.+(-\frac{25}{24}k_3-\frac{25}{48}k_2+\frac{25}{16}k_1)\cosh\left(\frac{5a_2}{2}\right)\right]p^B$$
$$+(-\frac{161}{512}k_3+\frac{75}{256}k_2+\frac{139}{512}k_1)\sinh\left(\frac{a_2}{2}\right)+(\frac{291}{64}k_3-\frac{675}{512}k_2+\frac{1803}{512}k_1)\sinh\left(\frac{3a_2}{2}\right)$$
$$\left.+(\frac{3775}{256}k_3+\frac{375}{512}k_2+\frac{8075}{512}k_1)\sinh\left(\frac{5a_2}{2}\right)\right\}$$
$$/k\left[2\cosh\left(\frac{a_2}{2}\right)e^{\frac{b_2}{4}}+2\cosh\left(\frac{3a_2}{2}\right)e^{\frac{9b_2}{4}}\right]$$

$$\Omega\frac{do^B}{d\xi}=$$
$$\left\{\left[-\frac{137}{480}(k_3-k_1)\sinh\left(\frac{a_2}{2}\right)-\frac{57}{5}(k_3-k_1)\sinh\left(\frac{3a_2}{2}\right)-\frac{4175}{48}(k_3+k_1)\sinh\left(\frac{5a_2}{2}\right)\right]m^B\right.$$
$$+\left[\frac{13}{12}(k_3-k_1)\sinh\left(\frac{a_2}{2}\right)+\frac{17}{3}(k_3-k_1)\sinh\left(\frac{3a_2}{2}\right)+\frac{221}{6}(k_3-k_1)\sinh\left(\frac{5a_2}{2}\right)\right]r^B$$

$$+\left[-(k_3+k_1)\cosh\left(\frac{a_2}{2}\right)-(k_3+k_1)\cosh\left(\frac{3a_2}{2}\right)-(k_3+k_1)\cosh\left(\frac{5a_2}{2}\right)\right]o^B \tag{2.20}$$

$$+\left[\frac{7}{30}(k_3-k_1)\sinh\left(\frac{a_2}{2}\right)-\frac{4}{15}(k_3-k_1)\sinh\left(\frac{3a_2}{2}\right)-\frac{11}{3}(k_3-k_1)\sinh\left(\frac{5a_2}{2}\right)\right]p^B \tag{2.21}$$

$$+\left[\frac{1}{16}(k_3+k_1)\cosh\left(\frac{a_2}{2}\right)+\frac{81}{16}(k_3+k_1)\cosh\left(\frac{3a_2}{2}\right)+\frac{625}{16}(k_3+k_1)\cosh\left(\frac{5a_2}{2}\right)\right]\Bigg\}$$

$$/k\left[2\cosh\left(\frac{a_2}{2}\right)e^{\frac{b_2}{4}}+2\cosh\left(\frac{3a_2}{2}\right)e^{\frac{9b_2}{4}}\right]$$

$$\Omega\frac{dp^B}{d\xi}=$$

$$\Bigg\{\Bigg[(\frac{1183}{15360}k_3-\frac{75}{512}k_2+\frac{1067}{15360}k_1)\cosh\left(\frac{a_2}{2}\right)+(-\frac{12069}{640}k_3+\frac{2025}{1024}k_2+\frac{86427}{5120}k_1)\cosh\left(\frac{3a_2}{2}\right)$$

$$+(-\frac{330625}{1536}k_3-\frac{1875}{1024}k_2+\frac{666875}{3072}k_1)\cosh\left(\frac{5a_2}{2}\right)\Bigg]m^B$$

$$+\Bigg[(-\frac{1019}{256}k_3-\frac{17}{384}k_2+\frac{3091}{768}k_1)\sinh\left(\frac{a_2}{2}\right)+(-\frac{1571}{96}k_3+\frac{3159}{256}k_2+\frac{3091}{768}k_1)\sinh\left(\frac{3a_2}{2}\right)$$

$$+(\frac{2089}{128}k_3-\frac{15625}{768}k_2-\frac{3091}{768}k_1)\sinh\left(\frac{5a_2}{2}\right)\Bigg]q^B$$

$$+\Bigg[(-\frac{23}{384}k_3+\frac{17}{192}k_2-\frac{11}{384}k_1)\cosh\left(\frac{a_2}{2}\right)+(\frac{243}{16}k_3-\frac{1053}{128}k_2-\frac{891}{128}k_1)\cosh\left(\frac{3a_2}{2}\right)$$

$$+(\frac{15625}{192}k_3+\frac{3125}{384}k_2-\frac{34375}{384}k_1)\cosh\left(\frac{5a_2}{2}\right)\Bigg]r^B$$

$$+\Bigg[(\frac{399}{128}k_3+\frac{1}{192}k_2-\frac{1199}{384}k_1)\sinh\left(\frac{a_2}{2}\right)+(\frac{241}{48}k_3-\frac{243}{128}k_2-\frac{1199}{384}k_1)\sinh\left(\frac{3a_2}{2}\right) \tag{2.21}$$

$$+(-\frac{321}{64}k_3+\frac{3125}{384}k_2-\frac{1199}{384}k_1)\sinh\left(\frac{5a_2}{2}\right)\Bigg]o^B$$

$$+\Bigg[(-\frac{953}{960}k_3-\frac{1}{96}k_2-\frac{319}{320}k_1)\cosh\left(\frac{a_2}{2}\right)+(-\frac{121}{40}k_3+\frac{81}{64}k_2-\frac{77}{320}k_1)\cosh\left(\frac{3a_2}{2}\right)$$

$$+(-\frac{721}{96}k_3-\frac{625}{192}k_2+\frac{561}{64}k_1)\cosh\left(\frac{5a_2}{2}\right)\Bigg]p^B$$

$$+(\frac{1639}{2048}k_3+\frac{75}{1024}k_2-\frac{1161}{2048}k_1)\sinh\left(\frac{a_2}{2}\right)+(\frac{2919}{256}k_3-\frac{6075}{2048}k_2+\frac{13827}{2048}k_1)\sinh\left(\frac{3a_2}{2}\right)$$

$$+(\frac{96175}{1024}k_3+\frac{9375}{2048}k_2+\frac{198275}{2048}k_1)\sinh\left(\frac{5a_2}{2}\right)\Bigg\}$$

$$/k\left[2\cosh\left(\frac{a_2}{2}\right)e^{\frac{b_2}{4}}+2\cosh\left(\frac{3a_2}{2}\right)e^{\frac{9b_2}{4}}\right],$$

where $a_1=(m^A+h_0\cos(\xi))/T,\ b_1=(\Bbbk\, q^B+\eth)/T,\ a_2=(m^A+h_0\cos(\xi))/T,\ b_2=(\Bbbk\, q^A+\eth)/T,$

$\mathbb{d} = -D/zJ$, $\mathbb{k} = K/z\,J$, $T = (\beta\ zJ)^{-1}$ and $\Omega = \omega/k$, $k = \frac{k_1}{k_2}$, $k_3 = \sqrt{k_1 k_2}$, $\xi = \omega t$, $h_0 = H_0/z\,J$ and z=4. Moreover, we fixed $k_1 = 1.0$ and $k_2 = 2.0$ in all numerical calculations due to the reason that most systems have longer relaxation times for the translation and shorter relaxation times for rotation. m^A, m^B, q^A and q^B give the dynamic features of the system, because of the behavior r^A, o^A are similar to the q^A, m^A, respectively and similarly the behavior r^B, o^B, p^B are similar to the q^B, m^B respectively. Therefore, we only investigate the behavior of m^A, m^B, q^A and q^B to study the dynamic multicritical phase diagrams of the mixed spin (2, 5/2) Blume-Emery-Griffiths model with the repulsive biquadratic coupling.

3. Numerical results and discussion

3.1. Phases in the system and the dynamic phase transitions

In this subsection, we obtained phases in the system by examining the average dynamic dipole moments (magnetizations, m^A, m^B) and quadrupole moments (q^A, q^B) order parameters, and by investigating the dynamic dipole moments (magnetizations, M^A, M^B) and quadrupole moments (Q^A, Q^B) order parameters. We also characterized the nature (first- or second-order) of dynamic phase transitions (DPTs) and obtained DPT temperatures by investigating the temperature dependence of the dynamic magnetizations and quadrupole moments order parameters. First, we should investigate the stationary solutions of the set of the average dynamical equations (Eqs. (2.14)-(2.17) and (2.18)-(2.21)), when the parameters T, h_0, $\mathbb{d}$ and $\mathbb{k}$ are varied. As we mentioned at the end of Section 2, we will only investigate the stationary solutions of the average dynamic magnetizations and quadrupoles order parameters. The stationary of m^A, m^B, q^A, q^B will be periodic functions of ξ with period 2π; that is,

$$m^A(\xi + 2\pi) = m^A(\xi) \text{ and } m^B(\xi + 2\pi) = mB(\xi), \tag{3.1}$$

$$q^A(\xi + 2\pi) = q^A(\xi) \text{ and } q^B(\xi + 2\pi) = qB(\xi). \tag{3.2}$$

Moreover, they can be one of three types according to whether they have or do not have the property

$$m^A(\xi + 2\pi) = -m^A(\xi) \text{ and } m^B(\xi + 2\pi) = -m^B(\xi), \tag{3.3}$$

$$q^A(\xi + 2\pi) = -q^A(\xi) \text{ and } q^B(\xi + 2\pi) = -q^B(\xi). \tag{3.4}$$

The first type of solution satisfying both Eqs. (3.3) and (3.4) is called a symmetric solution which corresponds to a disordered (d) solution or phase. In this symmetric solution, $m^A = m^B = 0.0$; hence magnetizations oscillate around zero and are delayed with respect to the external magnetic field. On the other hand, q^A oscillates around a zero or nonzero value, but q^B only around nonzero for finite temperature and both oscillate around zero for infinite temperature. The second type of solution is called a nonsymmetric solution that does not satisfy Eq. (3.3) and Eq. (3.4) that corresponds to a ferrimagnetic (i) solution or phase. In this solution or phase, $m^A \neq m^B$, and they oscillate around a nonzero value. We found the following six different ferrimagnetic phases: (1) If $m^A(\xi)$ and $m^B(\xi)$ oscillate around ± 2 and $\pm 5/2$, respectively, these solutions have been named the ferrimagnetic-I (i_1) phase. (2) If $m^A(\xi)$ and $m^B(\xi)$ oscillate around ± 2 and $\pm 3/2$, respectively, these solutions have been called the ferrimagnetic-II (i_2) phase. (3) If $m^A(\xi)$ and $m^B(\xi)$ oscillate around ± 2 and $\pm 1/2$,

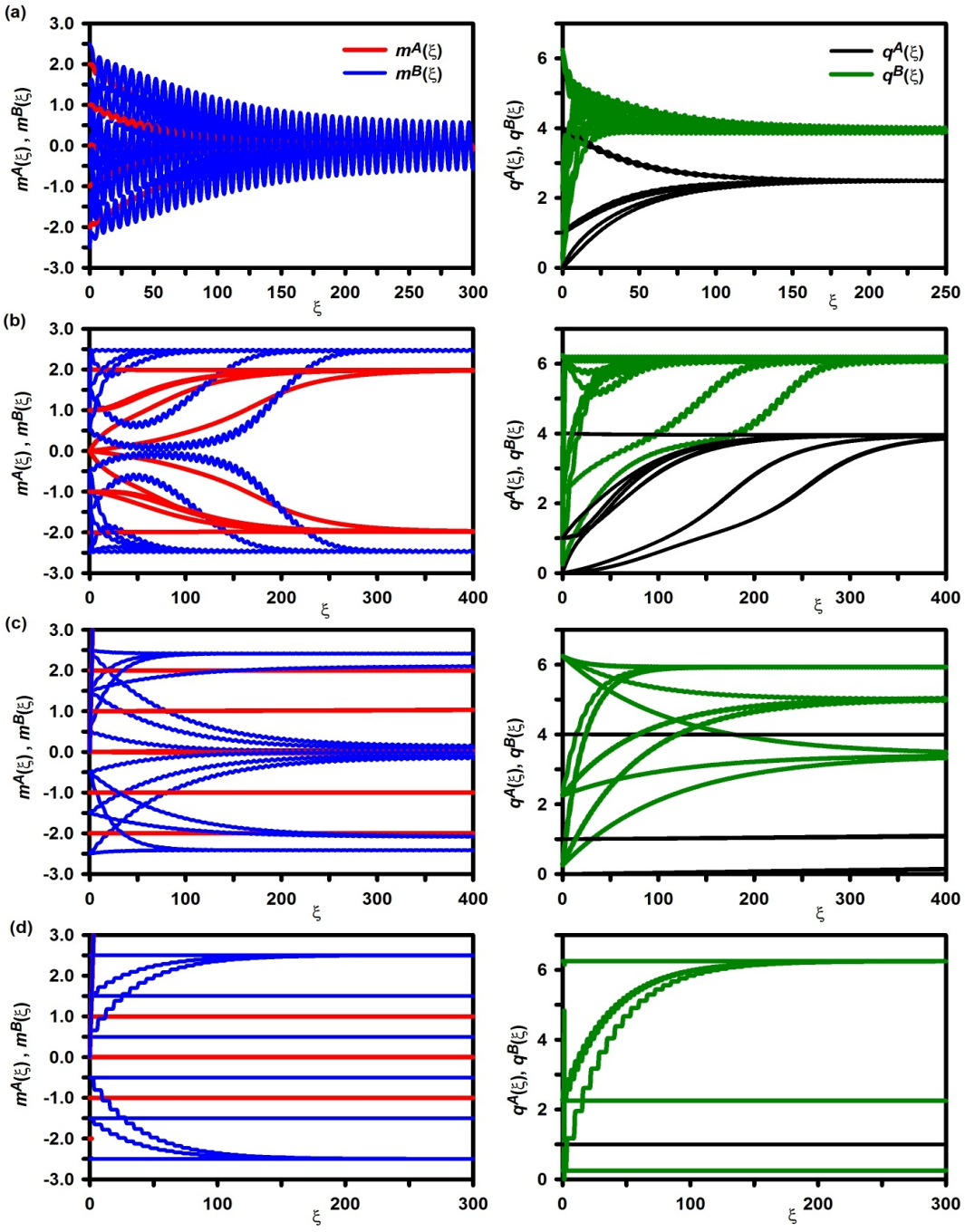

Figure 1. Time variations of average magnetizations (m^A, m^B) and quadrupole order parameters (q^A, q^B): **(a)** Exhibiting a disordered (d) phase for $\mathbb{k} = -0.10$, $\mathbb{d} = 1.75$, $h_0 = 1.75$, $T = 1.75$; **(b)** Illustrating a ferrimagnetic-I (i_1) phase for $\mathbb{k} = -0.10$, $\mathbb{d} = 1.00$, $h_0 = 0.55$, $T = 0.65$; **(c)** Displaying a mixed or hybrid ($a + i_1 + i_4$) phase for $\mathbb{k} = -0.025$, $\mathbb{d} = 1.75$, $h_0 = 0.50$, $T = 0.80$; **(d)** Illustrating a mixed ($i_4 + i_6 + nm_1 + nm_2 + nm_3$) phase for $\mathbb{k} = -0.10$, $\mathbb{d} = 1.00$, $h_0 = 1.00$, $T = 0.08$.

respectively, the solutions have been named the ferrimagnetic-III (i_3). (4) If $m^A(\xi)$ and $m^B(\xi)$ oscillate around ± 1 and $\pm 5/2$, respectively, the solutions have been named the ferrimagnetic-IV (i_4). (5) If $m^A(\xi)$ and $m^B(\xi)$ oscillate around ± 1 and $\pm 3/2$, respectively, the solutions have been called the ferrimagnetic-V (i_5) phase. (6) If $m^A(\xi)$ and $m^B(\xi)$ oscillate around ± 1 and $\pm 1/2$, respectively, the solutions have been named the ferrimagnetic-VI (i_6). The quadrupole order parameters q^A and q^B are not equal to each other, and they oscillate around a nonzero value. In this case, the magnetization and quadrupole order parameters do not follow the external magnetic field.

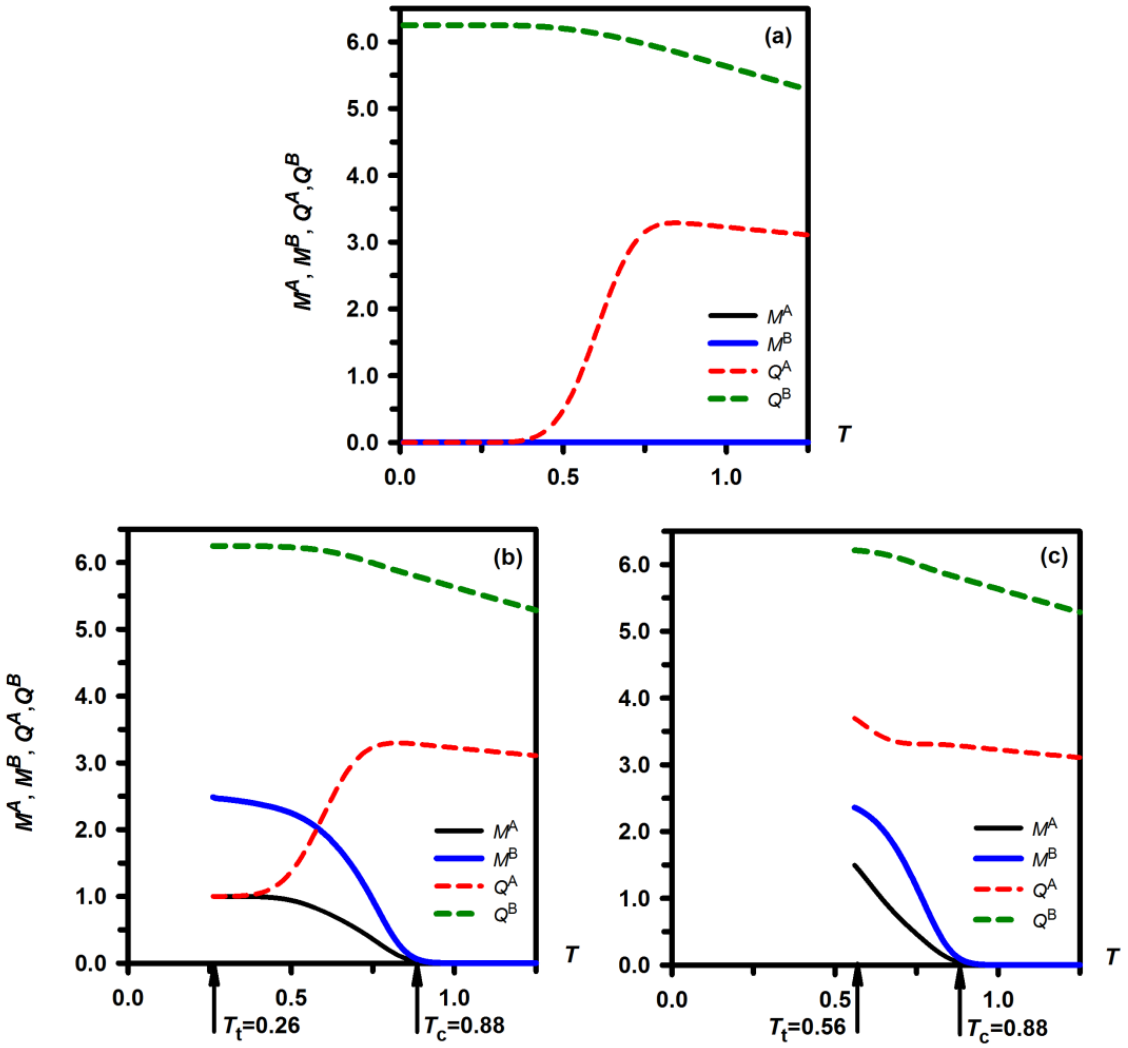

Figure 2. The thermal behavior of dynamic magnetizations (M^A, M^B) and the dynamic quadrupole order parameters (Q^A, Q^B) for $\Bbbk = -0.025$, $\mathbb{d} = 1.25$, $h_0 = 2.80$, and different initial values. The thin (black) and thick (blue) lines, respectively, represent M^A and M^B, and the thick dashed (green) and thin dashed (red) lines represent Q^A and Q^B, respectively. T_c and T_t are the second- and first-order phase transition temperatures for the dynamic order parameters, respectively. It illustrates that the system first passes from the d phase to the i_4 phase at $T_{t1} = 0.26$ and then the i_4 phase to the $i_1 + i_4$ mixed phase at $T_{t2} = 0.56$, and finally from the $i_1 + i_4$ to the d phases at $T_c = 0.88$.

On the other hand, if $m^A(\xi)$ oscillates around zero, but and $m^B(\xi)$ around nonzero, these indicate that nonmagnetic phases occur in the system. The following three nonmagnetic phases were found: The nonmagnetic phase-II (nm_1), $m^A(\xi)$ and $m^B(\xi)$ oscillate around a zero and $\pm 5/2$ values, respectively, the nonmagnetic phase-II (nm_2), $m^A(\xi)$ and $m^B(\xi)$ oscillate around a zero and $\pm 3/2$ values, respectively and the nonmagnetic phase-III (nm_3), $m^A(\xi)$ and $m^B(\xi)$ oscillate around a zero and $\pm 1/2$ values, respectively.

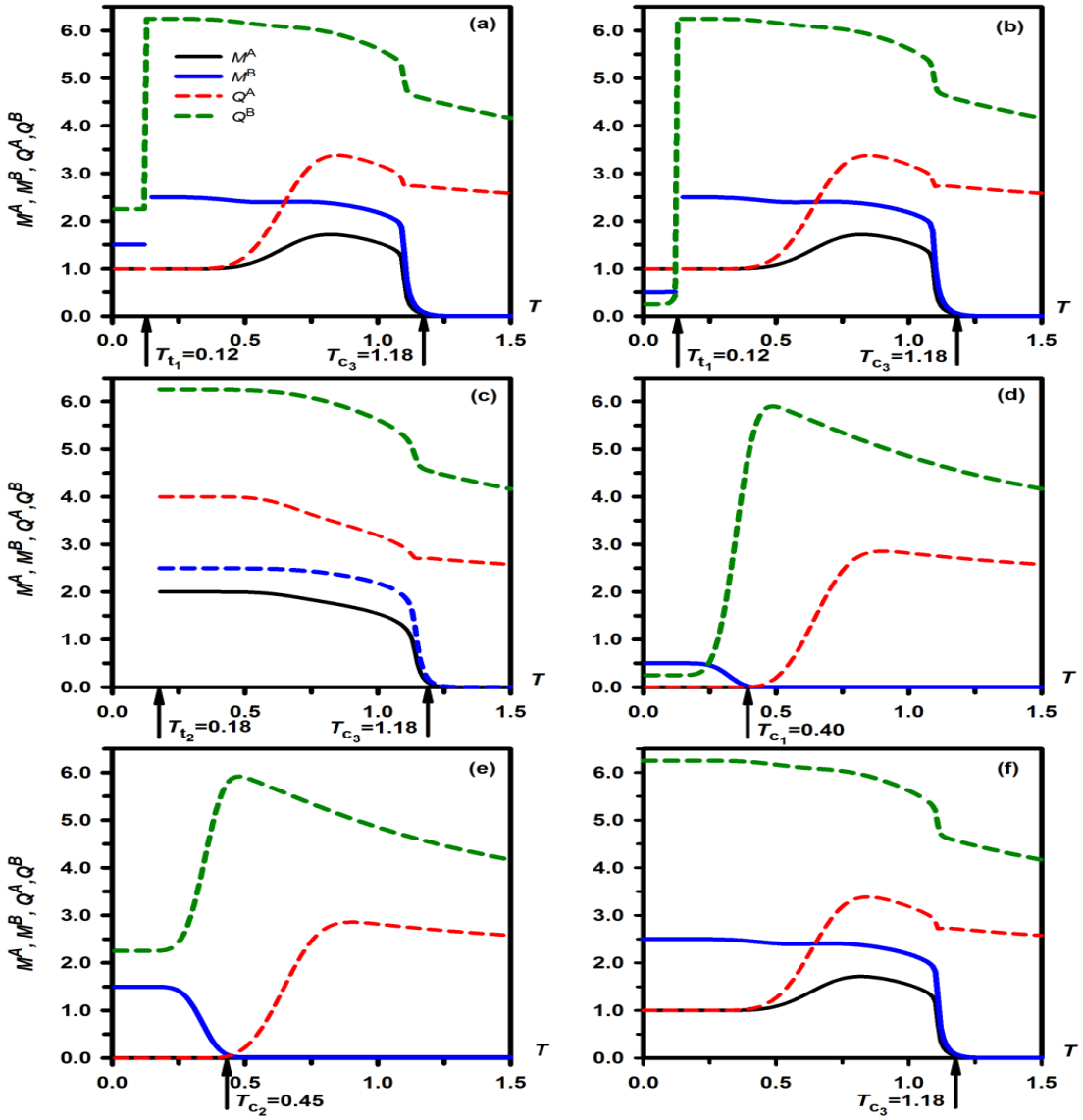

Figure 3. Same as Figure 2, but for $\Bbbk = -0.025$, $\mathrm{d} = 1.75$, $h_0 = 1.75$, and different initial values. Exhibiting the system first undergoes from the $i_4 + i_5 + i_6 + nm_2 + nm_3$ mixed phase to the $i_4 + nm_2 + nm_3$ mixed phase at $T_{t1} = 0.12$, then the $i_4 + nm_2 + nm_3$ to the phases at $T_{t2} = 0.18$, and then from the $i_4 + i_1 + nm_2 + nm_3$ mixed phase to the $i_4 + i_1 + nm_2$ hybrid phase at $T_{c1} = 0.40$, and the $i_4 + i_1 + nm_2$ to the $i_4 + i_1$ phases at $T_{c2} = 0.45$, finally the $i_4 + i_1$ phase to the d phase at $T_{c3} = 1.18$.

The quadrupole order parameters q^A and q^B are not equal to each other, and they oscillate around a nonzero value. The third type of solution, which satisfies Eq. (3.3) but does not satisfy Eq. (3.4), corresponds to the antiquadrupolar or staggered solution or phase (a). In this solution, $m^A = m^B = 0.0$; m^A and m^B oscillate around zero value and are delayed respect the external magnetic field. The quadrupole order parameters q^A and q^B are not equal to each other and they oscillate around a nonzero value for always finite temperature. The definitions of these fundamental phases are given in Table A.1.

In addition to these fundamental phases, we obtained various different mixed or hybrid phases, such as $i_4+i_5+i_6+nm_2+nm_3$, $i_1+i_4+nm_2+nm_3$, $\mathrm{i}_4+nm_2+nm_3$, ..., $a+i_4+i_1$, i_4+i_1, etc., by numerically solving Eqs. (2.14)-(2.17) and (2.18)-(2.21) as well as investigating the thermal behaviors of average dynamic magnetizations. All mixed phases occurring in the system are given in Table B.1. We plotted only four exploratory figures to illustrate the d, i_1 fundamental phases and the $a+i_4+i_1$ and $i_4+i_6+nm_1+nm_2+nm_3$ hybrid or mixed phases, seen in Figure 1 (panels a-d) for various values of system parameters. It can be easily understood from the explanations given above in which Figure 1 a,b,c and d panels illustrate the disordered (d), ferrimagnetic-I (i_1) fundamental phases, the $a+i_1+i_4$ and $i_4+i_6+nm_1+nm_2+nm_3$ mixed phases, respectively. It is worth mentioning that only the d, i_1 and i_4 fundamental phases separately occur in the dynamic phase diagrams (DPDs) and the other fundamental phases occurs inside the mixed or hybrid phases. These facts are clearly seen in the DPDs, namely in Figures 4 and 5. We should also mention that some mixed phases are obtained very easily from the numerical solution of Eqs. (2.12) and (2.13). The some of them are very difficult to obtained from these equations in which these mixed phases were found by the help of investigating the thermal behaviors of the dynamic magnetizations (M^A, M^B) and quadrupole moment order parameters (Q^A, Q^B), given below.

Table 1. The description of the rate constants for the sublattices A and B.

(a) For sublattice A.

	X$_1$(2)	X$_2$(1)	X$_3$(0)	X$_4$(-1)	X$_5$(-2)
X$_1$(2)		k_1	k_1	k_3	k_2
X$_2$(1)	k_1		k_1	k_2	k_3
X$_3$(0)	k_1	k_1		k_1	k_1
X$_4$(-1)	k_3	k_2	k_1		k_1
X$_5$(-2)	k_2	k_3	k_1	k_1	

(b) For sublattice B.

	X$_1$(5/2)	X$_2$(3/2)	X$_3$(1/2)	X$_4$(-1/2)	X$_5$(-3/2)	X$_6$(-5/2)
X$_1$(5/2)		k_1	k_1	k_3	k_3	k_2
X$_2$(3/2)	k_1		k_1	k_3	k_2	k_3
X$_3$(1/2)	k_1	k_1		k_2	k_3	k_3
X$_4$(-1/2)	k_3	k_3	k_2		k_1	k_1
X$_5$(-3/2)	k_3	k_2	k_3	k_1		k_1
X$_6$(-5/2)	k_2	k_3	k_3	k_1	k_1	

We also investigated the behavior of the dynamic magnetizations (M^A, M^B) and the dynamic quadrupole order parameters (Q^A, Q^B) as functions of the reduced temperature. These investigations lead us to define nature (first- or second-order) of the dynamic phase transition (DPT) and to obtain the DPT points as well as to observe the phases, especially mixed phases that cannot be obtained from Eqs. (2.12) and (2.13). Thus, M^A, M^B and Q^A, Q^B can be defined as

$$M^A = \frac{1}{2\pi}\int_0^{2\pi} m^A(\xi)d\xi \text{ and } M^B = \frac{1}{2\pi}\int_0^{2\pi} m^B(\xi)d\xi, \tag{3.5}$$

and similarly,

$$Q^A = \frac{1}{2\pi}\int_0^{2\pi} q^A(\xi)d\xi \text{ and } Q^B = \frac{1}{2\pi}\int_0^{2\pi} q^B(\xi)d\xi. \tag{3.6}$$

Eqs. (3.5) and (3.6) were solved by using the Adams-Moulton predictor corrector method with Romberg integration. A few exploratory and interesting results are plotted for several values of system parameters and initial values in Figures 2 and 3. In these figures, the thin (black) and thick (blue) lines represent M^A and M^B, respectively, and the thick dashed (green) and thin dashed (red) lines represent Q^A and Q^B, respectively. T_t and T_c, respectively, indicate the dynamic first-order phase transition (FOPT) and second-order phase transition (SOPT) temperatures. Figure 2 was obtained for $\Bbbk = -0.025$, $\mathbb{d} = 1.25$, $h_0 = 2.80$ and different initial values. This figure displays that the system first undergoes the FOPT at $T_{t1} = 0.26$ from the d phase (Figure 2 panel (a)) to the i_4 (Figure 2 panel (b)) phase, the reason that discontinuous occurs on M^A, M^B, and then the i_4 phase to the $i_1 + i_4$ (Figure 2 panel (c)) hybrid phase at $T_{t2} = 0.56$ and finally the system undergoes the SOPT from the $i_1 + i_4$ mixed phase to the d phase at $T_c = 0.88$, the reason that M^A and M^B become zero continuously. Thus, one can evidently observe that the $i_1 + i_4$ mixed or hybrid phase occurs between T_{t2} and T_c, and also very clearly seen in Figure 4 panel (c) for $h_0 = 2.80$. Figure 3 was plotted for $\Bbbk = -0.100$, $\mathbb{d} = 1.75$, $h_0 = 1.75$ and different initial values in which exhibits more interesting and complex behaviors. The system first undergoes the FOPT at $T_{t1} = 0.12$ from the $i_4 + i_5 + i_6 + nm_2 + nm_3$ hybrid phase to the $i_4 + nm_2 + nm_3$ mixed phase (Figures 3a and 3d-3f), then the $i_4 + nm_2 + nm_3$ to the$i_4 + i_1 + nm_2 + nm_3$ phases at $T_{t2} = 0.18$ (Figures 3b and 3d-3f), and then from the $i_4 + i_1 + nm_2 + nm_3$ mixed phase to the $i_4 + i_1 + nm_2$ hybrid phase at $T_{C1} = 0.40$ (Figures 3c and 3d-3f), and the$i_4 + i_1 + nm_2$ to the $i_4 + i_1$ phases at $T_{C2} = 0.45$ (Figures 3d-3f), finally the $i_4 + i_1$ mixed phase to the d phase at $T_{C3} = 1.18$ (Figures 3c and 3f). On the other hand, Q^A and Q^B make a sharp or a smooth cusp at T_t and T_c.

3.2. Dynamic phase diagrams

Since we found the phases, characterized nature of DPTs, and obtained the DPT temperatures, we can now present the dynamic phase diagrams (DPDs) of the system. The calculated phase diagrams in the (T, h_0) plane are presented for various values of $\Bbbk$ and $\mathbb{d}$, seen in Figures 4 and 5. In these figures, the dashed (blue) and solid (red) lines, respectively, indicate the FOPT and SOPT lines. TCP, B, E, IE, Z, and QP represent the dynamic tricritical point, double critical end point, critical end point, inverse critical end point (termination of first-order phase lines at the critical point), zero critical end point and quadruple point (the point where two different first-order phase lines intersect), respectively.

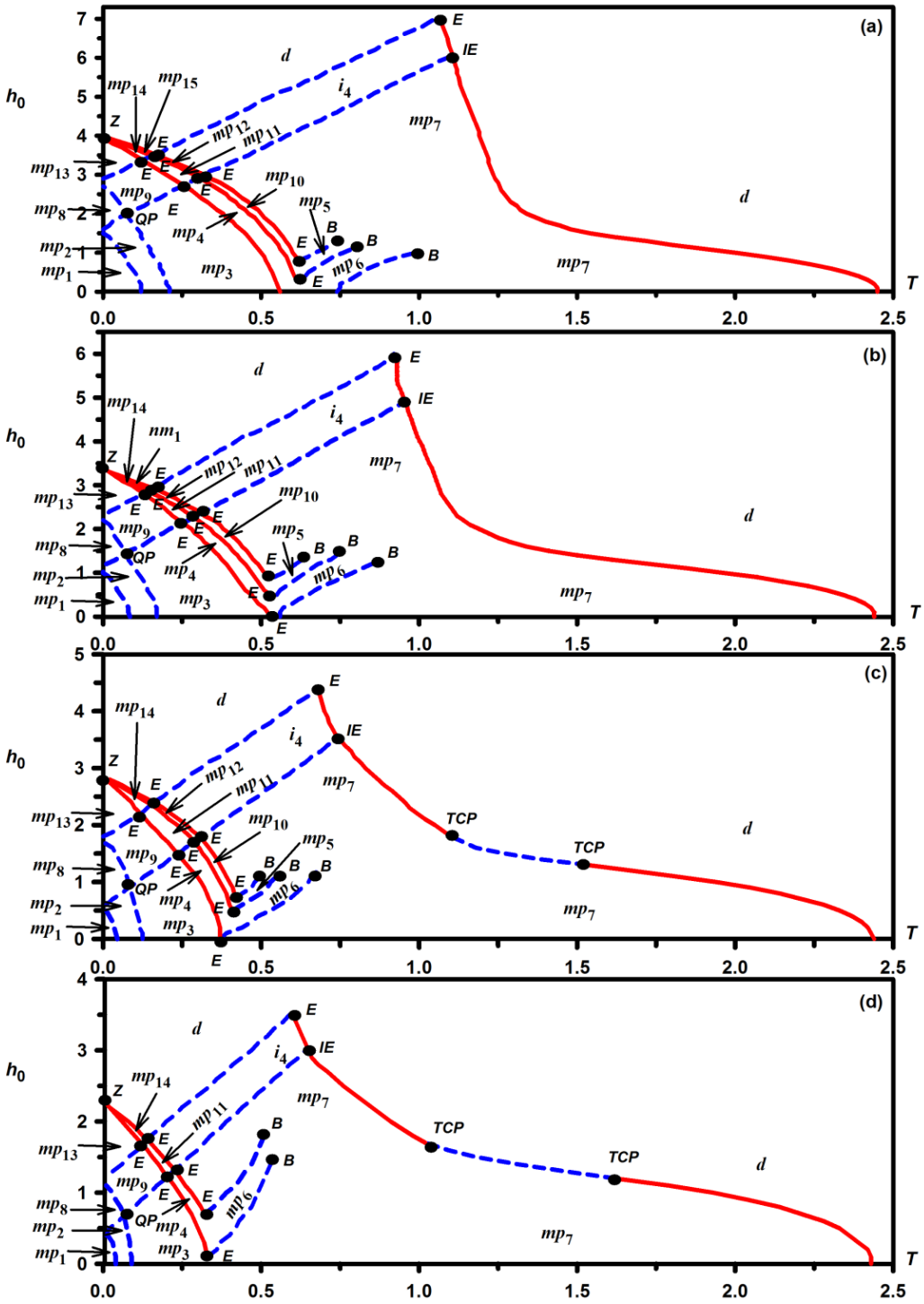

Figure 4. The dynamic phase diagrams in the (T, h_0) plane. Solid (red) and dashed (blue) lines, respectively, indicate the second- and first-order phase transition lines. TCP, B, E, IE, Z, and QP represent the dynamic tricritical point, double critical end point, critical end point, inverse critical end point, zero critical end point and quadruple point, respectively. Definitions of fundamental and mixed (mp_i) phases are given Tables A.1 and B.1, respectively. **(a)** $\mathbb{k} = -0.025$ and $\mathbb{d} = 1.75$, **(b)** $\mathbb{k} = -0.025$ and $\mathbb{d} = 1.50$, **(c)** $\mathbb{k} = -0.025$ and $\mathbb{d} = 1.25$, and **(d)** $\mathbb{k} = -0.025$ and $\mathbb{d} = 1.00$.

Figure 4a was obtained for $\mathbb{k} = -0.025$ and $\mathbb{d} = 1.75$, and the following interesting and important phenomena were observed from this figure: (1) It displays nine E, three B, one Z, IE and QP dynamic critical points. (2) Beside the disordered phase (d), one ferrimagnetic (i_4) phase and one nonmagnetic (nm_2) fundamental phase, up to fifteen different mixed phases occur in the system. (3) DPD does not exhibit the dynamic TCR point behavior. (4) The more complicated mixed phases mostly occur for small values of T and h_0. (5) The dynamic FOPT boundaries among the mixed phases are more than the SOPT boundaries. (6) The areas of the mp_{14}, and mp_{15} mixed phases becomes smaller as T and h_0 getting smaller and they disappeared at $T = 0$. (8) The system also displays the reentrant behavior, i.e. as T is increased, the system undergoes from the d phase the $i_1 + i_4$ mixed phase and back to the d phase again. (9) The boundaries between the d and the mixed phases are the SOPT lines for high and very low values of T, but the FOPT lines for intermediate T values. Figure 4b was plotted for $\mathbb{k} = -0.025$ and $\mathbb{d} = 1.50$ that is like to Figure 4a, except three following differences: (1) One more critical end point (E) occurs for small values of T and $h_0 = 0.0$. (2) The FOPT and SOPT lines and all the special dynamic critical points consist for lower values of h_0 and T. (3) The mp_{15} mixed phase becomes the nm_1 fundamental phase. Figures 4c was constructed for $\mathbb{k} = -0.025$ and $\mathbb{d} = 1.25$, and it is similar to Figure 4b, except followings: Two dynamic $TCPs$ emerge for the low value of h_0 and high value of T, and the nm_1 fundamental phase disappears; hence, one of E also vanishes. Moreover, the special dynamic critical points, and the FOPT and SOPT lines take place for more small values of h_0 and T. Figure 4d was obtained for $\mathbb{k} = -0.025$ and $\mathbb{d} = 1.00$ and it is similar to Figure 4c, apart from following distinctions. (1) The SOPT line that observed at high values of T and h_0 disappears; hence two E and one B special dynamic critical points, and the mp_{12} and mp_{10} mixed phase vanish. (2) The FOPT line that observed for high values of T and h_0 disappears; hence, the mp_5 mixed phase disappear. Moreover, the dynamic FOPT lines between two dynamic $TCPs$ become longer as $\mathbb{d}$ values decreasing.

We also constructed the DPDs for higher values of the repulsive biquadratic coupling $(\mathbb{k})$ and various values of $\mathbb{d}$, seen in Figure 5. Figure 5a was obtained for $\mathbb{k} = -0.100$ and $\mathbb{d} = 1.75$ that is like Figure 4a, except the following four important differences. (1) SOPT line that emerged at low values of T and h_0, and the FOPT line observed for lower values of T and higher values of h_0 disappears; thus, three E and one B special dynamic critical points, and four mixed phases are lost. (2) FOPT and SOPT lines as well as all the special dynamic critical points occur for lower values of T and h_0. (3) The components of mixed phases are different. (4) The nm_2 phase is observed instead of the nm_1 phase as a separate single phase. Figure 5b was plotted for $\mathbb{k} = -0.100$ and $\mathbb{d} = 1.75$ and it is similar to Figure 5a, only differences illustrate dynamic tricritical behaviors; hence, two dynamic $TCPs$ occurs, and one more E point emerges for the low value of h_0. Figure 5c was constructed for $\mathbb{k} = -0.100$ and $\mathbb{d} = 1.25$ in which similar to Figure 5b, except the following differences. (1) One more SOPT line occurs for smaller values of T and h_0. (2) One more FOPT line is observed for higher values of T. (3) Two more B and one more E special critical points emerge, and the FOPT and SOPT lines as well as all the special dynamic critical points occur for more small values of T and h_0. (4) Few more number of mixed phases was observed. (5) The components of mixed phases also change. (6) Then m_2 fundamental phase turns into the mp_{14} mixed phase. Finally, Figure 5d was found for $\mathbb{k} = -0.100$ and $\mathbb{d} = 1.00$ and it is like to Figure 5c, except the FOPT line that terminates at the IE disappears; hence, some of the mixed phases disappear, and the combinations of mixed phases are different. Moreover, the i_1 is observed instead of the $mp_7(i_1 + i_4)$ mixed phase.

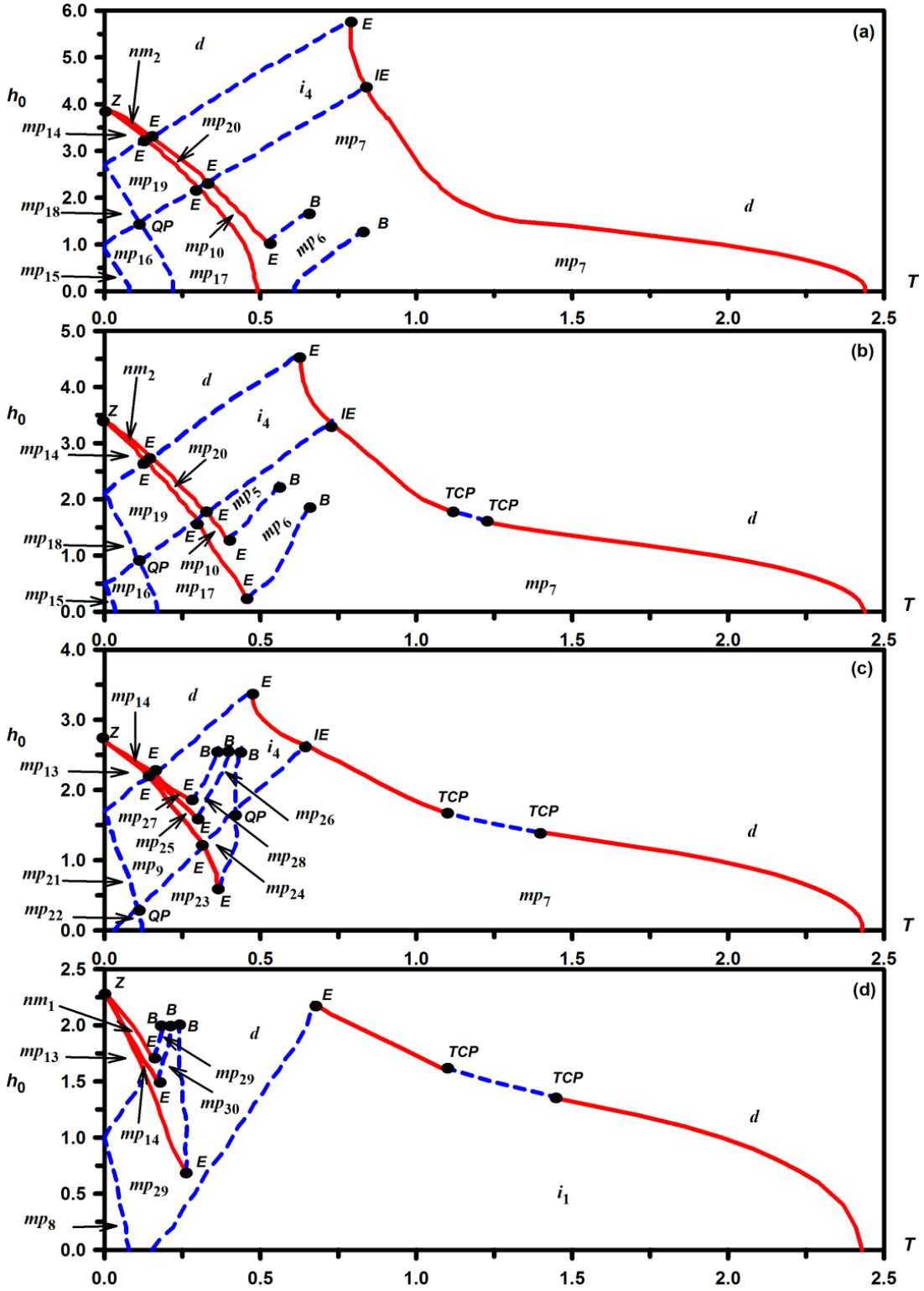

Figure 5. Same as Figure 4, but **(a)** $\mathbb{k} = -0.10$ and $\mathbb{d} = 1.75$, **(b)** $\mathbb{k} = -0.10$ and $\mathbb{d} = 1.50$, **(c)** $\mathbb{k} = -0.10$ and $\mathbb{d} = 1.25$, and **(d)** $\mathbb{k} = -0.100$ and $\mathbb{d} = 1.00$.

Finally, we should also mention that very recently the similar DPDs were obtained in the mixed spin (2, 5/2) Blume-Capel model [33], but the DPDs of Figures 4 and 5 illustrate more richer and interesting dynamic critical phenomena.

4. Summary and conclusion

We investigated the DPTs and presented the DPDs of a mixed spin (2, 5/2) BEG model in the presence of an oscillating magnetic field. We utilized the PPM to find the set average of dynamic order parameters as well as dynamic order parameters. We numerically solved these dynamic equations to find the phases in the system as well as to characterize the nature of DPTs and find DPT points. We constructed the DPDs in the (T, h_0) plane for various values of the repulsive biquadratic ($\mathbb{k}$) nearest-neighbor interaction and crystal-field interaction ($\mathbb{d}$). We observed that the system illustrates very rich and interesting topological behaviors of DPDs, such as up to two dynamic tricritical points, eight critical end points, three double critical end points, a zero-temperature critical point, one inverse critical end point and a quadruple point depending on interaction parameters. The system also shows the disordered, antiquadrupolar or staggered, three different nonmagnetic, and six different ferrimagnetic phases as well as various distinct mixed or hybrid phases. The system always exhibits the reentrant behavior for higher values of h_0 and lower values of T. The system does not illustrate the dynamic tricritical behavior for bigger values $\mathbb{d}$; hence, the dynamic tricritical behavior depend on the values of $\mathbb{d}$. We found that the number of mixed phases formed in the system as well as the components of the mixed phases occurred in the phase regions are highly dependent on the $\mathbb{k}$ and $\mathbb{d}$ values.

For higher values of h_0 and lower values of T, the i_1 fundamental phases appear as a separate single phase, and the IE special critical point disappears for smaller values of $\mathbb{k}$ and higher values $\mathbb{d}$. Lastly, we hope that our detailed theoretical investigations may stimulate further works to study to the DPTs and DPDs in different system within the PPM. We also hope that this work might shed some light to experimental scientists working on one of the currently growing and important subjects in the condensed matter physics.

Acknowledgment

This research was supported by The Scientific and Technical Research Council of Turkey (TÜBİTAK), grant no. 119F129.

References

[1] W. Jiang, W. Wang, F. Zhang, W. J. Ren, "Magnetic properties of a molecular-based magnet $AFe^{II}Fe^{III}(C_2O_4)_3$ with biaxial crystal field," *Journal of Applied Physics* **105** (2009) 07E321.

[2] C. Mathonière, C. J. Nuttall, S. G. Carling, P. Day, "Ferrimagnetic Mixed-Valency and Mixed-Metal Tris(oxalato)iron(III) Compounds: Synthesis, Structure, and Magnetism," *Inorg. Chem.* **35** (1996) 1201.

[3] Y. Nakamura, "Existence of a compensation temperature of a mixed spin-2 and spin-5/2 Ising ferrimagnetic system on a layered honeycomb lattice," *Physical Review B* **62** (2000) 111742.

[4] J. Li, A. Du, G. Z. Wei, "The Compensation Behavior of a Mixed-Spin-2 and Spin-5/2 Heisenberg Ferrimagnetic System on a Honeycomb Lattice," *Physica B* **348** (2004) 79.

[5] W. Jiang, V. C. Lo, B. D. Bai, J. Yang, "Magnetic hysteresis loops in molecular-based magnetic materials $AFe^{II}Fe^{III}(C_2O_4)_3$," *Physica A* **389** (2010) 2227.

[6] W. Wang, W. Jiang, D. Lv, "Monte Carlo Simulation of Layer Thickness Influence on a Mixed Spin-2 and Spin-5/2 Ising Ferrimagnetic System," *IEEE Transactions on Magnetics* **47** (2011) 3943.

[7] Y. Nakamura, S. Shin, T. Kaneyosh, "The effects of transverse field on the magnetic properties in a diluted mixed spin-2 and spin-5/2 Ising system," *Physica B: Condensed Matter* **284-288** (2000) 1479.

[8] S. Benyoussef, Y. EL Amraoui, H. Ez-Zahraouy, D. Mezzane, Z. Kutnjak et al., "Mean field theory and Monte Carlo simulation of phase transitions and magnetic properties of a tridimensional Fe_7S_8 compound," *Physica Scripta* **95** (2020) 045803.

[9] K. Chandran, P. Neenu Lekshmi, P. N. Santhosh, "High temperature spin reorientation, magnetization reversal and magnetocaloric effect in 50% Mn substituted polycrystalline $ErFeO_3$," *Journal of Solid State Chemistry* **279** (2019) 1120910.

[10] X. Shi, J. Zhao, L. Wang, X. Xu, "Compensation behaviors in the diluted $Fe^{II}Fe^{III}$ bimetallic oxalates," *Journal of Magnetism and Magnetic Materials* **452** (2018) 477.

[11] W. Hoston, A. N. Berker, "Dimensionality effects on the multicritical phase diagrams of the Blume–Emery–Griffiths model with repulsive biquadratic coupling: Mean-field and renormalization-group studies," *Journal of Applied Physics* **70** (1991) 6101.

[12] W. Hoston, A. N. Berker, "Multicritical phase diagrams of the Blume-Emery-Griffiths model with repulsive biquadratic coupling," *Physical Review Letters* **67** (1991) 1027.

[13] R. R. Netz, A. N. Berker, "Renormalization-group theory of an internal critical-end-point structure: The Blume-Emery-Griffiths model with biquadratic repulsion," *Physical Review B* **47** (1993) 15019.

[14] S. Lapinskas, A. Rosengren, "Blume-Emery-Griffiths model on three-dimensional lattices: Consequences for the antiferromagnetic Potts model," *Physical Review B* **49** (1994) 15190.

[15] A. Bakchich, M. El Bouziani, "Phase diagrams of the three-dimensional semi-infinite Blume-Emery-Griffiths model," *Physical Review B* **56** (1997) 11155.

[16] N. S. Branco, "Blume-Emery-Griffiths model on the square lattice with repulsive biquadratic coupling," *Physica A: Statistical Mechanics and its Applications* **232** (1996) 477.

[17] C. Ekiz, M. Keskin, "Multicritical phase diagrams of the Blume-Emery-Griffiths model with repulsive biquadratic coupling including metastable phases," *Physical Review B* **66** (2002) 054105.

[18] Ü. Temizer, E. Kantar, M. Keskin, O. Canko, "Multicritical dynamical phase diagrams of the kinetic Blume–Emery–Griffiths model with repulsive biquadratic coupling in an oscillating field," *Journal of Magnetism and Magnetic Materials* **320** (2008) 1787.

[19] A. Bakchich, M. El Bouziani, "Position-space renormalization-group investigation of the spin-3/2 Blume-Emery-Griffiths model with repulsive biquadratic coupling," *Journal of Physics: Condensed Matter* **13** (2001) 91.

[20] M. Keskin, O. Canko, "Multicritical phase diagrams of the ferromagnetic spin-3/2 Blume–Emery–Griffiths model with repulsive biquadratic coupling including metastable phases: The cluster variation method and the path probability method with the point distribution," *Journal of Magnetism and Magnetic Materials* **320** (2008) 8.

[21] Ç. Yunus, B. Renklioğlu, M. Keskin, A. N. Berker, "Stepwise positional-orientational order and the multicritical-multistructural global phase diagram of the s=3/2 Ising model from renormalization-group theory," *Physical Review E* **93** (2016) 062113.

[22] B. Deviren, M. Keskin, O. Canko, "Dynamic phase transition and multicritical dynamic phase diagrams of the kinetic spin-3/2 Blume–Emery–Griffiths model with repulsive biquadratic coupling under a time-dependent oscillating external field," *Computer Physics Communications* **178** (2008) 420.

[23] M. Keskin, E. Kantar, O. Canko, "Kinetics of a mixed spin-1 and spin-3/2 Ising system under a time-dependent oscillating magnetic field," *Physical Review E* **77** (2008) 051130.

[24] E. Albayrak, "Mixed spin-2 and spin-5/2 Blume–Emery–Griffiths model," *PPhysica A: Statistical Mechanics and its Applications* **375** (2007) 174.

[25] M. Ertaş, M. Keskin, B. Deviren, "Multicritical Dynamic Phase Diagrams and Dynamic Hysteresis Loops in a Mixed Spin-2 and Spin-5/2 Ising Ferrimagnetic System with Repulsive Biquadratic Coupling: Glauber Dynamic Approach," *Journal of Statistical Physics* **146** (2012) 1244.

[26] R. Kikuchi, "The Path Probability Method," *Progress of Theoretical Physics Supplement* **35** (1966) 1.

[27] J. L. Morán-López, J. M. Sanchez *(Eds.)*, "Theory and Applications of the Cluster Variation and Path Probability Methods," Plenum Press, New York, (1996).

[28] M. Özer, R. Erdem, "Dynamics of voltage-gated ion channels in cell membranes by the path probability method," *Physica A: Statistical Mechanics and its Applications* **331** (2004) 51.

[29] R. Yamada, T. Mohri, "Atomistic relaxation process in a Ni_3Al ordered phase using path probability method with vacancy mechanisms," *Computational Materials Science* **167** (2019) 118.

[30] R. Erdem, S. Özüm, "Relaxation times obtained from the rate equations using path probability method for the spin-1 Ising model," *Modern Physics Letters B* **33** (2019) 1950258.

[31] R. Yamada, T. Mohri, "Application of Cluster Variation and Path Probability Methods to the Tetragonal–Cubic Phase Transition in ZrO_2," *Journal of the Physical Society of Japan* **88** (2019) 074005.

[32] M. Gençaslan, M. Keskin, "Dynamic magnetic hysteresis loop features of molecular-based magnetic materials and ferrimagnetic systems by the path probability method," *Journal of Magnetism and Magnetic Materials* **514** (2020) 167242.

[33] M. Gençaslan, M. Keskin, "Nonequlibrium magnetic features in a mixed spin (2, 5/2) Ising system driven by the external oscillating magnetic field by path probability method," *Physica Scripta* **97** (2022) 085803.

Appendix

A. Definition of fundamental phases

Table A.1. The names, symbols and meanings of the fundamental phases observed in the system.

Fundamental phases	**Symbol**	**Definitions**
Disordered phase	d	$m^A = m^B = 0.0;\ q^A \geq 0.0,\ q > 0.0,$ and $q^A = q^B = 0.0$ at $T \to \infty$
Antiquadrupolar or staggered phase	a	$m^A = m^B = 0.0$ and $q^A \neq q^B > 0.0$
Nonmagnetic phase I	nm_1	$m^A = 0.0,\ m^B = \pm 5/2,$ and $q^A \neq q^B > 0.0$
Nonmagnetic phase II	nm_2	$m^A = 0.0,\ m^B = \pm 5/2,$ and $q^A \neq q^B > 0.0$
Nonmagnetic phase III	nm_3	$m^A = 0.0,\ m^B = \pm 1/2,$ and $q^A \neq q^B > 0.0$
Ferrimagnetic phase - I	i_1	$m^A = \pm 2.0,\ m = \pm 5/2,$ and $q^A \neq q^B > 0.0$
Ferrimagnetic phase - II	i_2	$m^A = \pm 2.0,\ m = \pm 3/2,$ and $q^A \neq q^B > 0.0$
Ferrimagnetic phase - III	i_3	$m^A = \pm 2.0,\ m = \pm 1/2,$ and $q^A \neq q^B > 0.0$
Ferrimagnetic phase - IV	i_4	$m^A = \pm 1.0,\ m = \pm 5/2,$ and $q^A \neq q^B > 0.0$
Ferrimagnetic phase - V	i_5	$m^A = \pm 1.0,\ m = \pm 3/2,$ and $q^A \neq q^B > 0.0$
Ferrimagnetic phase - VI	i_6	$m^A = \pm 1.0,\ m = \pm 1/2,$ and $q^A \neq q^B > 0.0$

B. Definition of mixed phases

Table B.1. The symbols and meanings of the mixed or hybrid phases observed in the system.

Symbols	Definitions
mp_1	$i_1 + i_2 + i_3 + i_4 + i_5 + i_6 + nm_1 + nm_2 + nm_3$
mp_2	$i_1 + i_4 + i_5 + i_6 + nm_1 + nm_2 + nm_3$
mp_3	$i_1 + i_4 + nm_1 + nm_2 + nm_3$
mp_4	$i_1 + i_4 + nm_1 + nm_2 + d$
mp_5	$i_1 + i_4 + a$
mp_6	$i_1 + i_4 + d$
mp_7	$i_1 + i_4$
mp_8	$i_4 + i_6 + nm_1 + nm_2 + nm_3$
mp_9	$i_4 + nm_1 + nm_2 + nm_3$
mp_{10}	$i_1 + i_4 + nm_1 + d$
mp_{11}	$i_4 + nm_1 + nm_2$
mp_{12}	$i_4 + nm_1$
mp_{13}	$nm_1 + nm_2 + nm_3$
mp_{14}	$nm_1 + nm_2$
mp_{15}	$i_1 + i_2 + i_3 + i_4 + i_5 + i_6 + nm_1$
mp_{16}	$i_1 + i_4 + i_5 + i_6 + nm_1$
mp_{17}	$i_1 + i_4 + nm_1$
mp_{18}	$i_4 + i_5 + i_6 + nm_2 + nm_3$
mp_{19}	$i_4 + nm_2 + nm_3$
mp_{20}	$i_1 + i_4 + nm_2$
mp_{21}	$i_4 + i_5 + i_6 + nm_3$
mp_{22}	$i_1 + i_5 + i_6$
mp_{23}	$i_1 + i_4 + nm_3$
mp_{24}	$nm_2 + nm_3 + d$
mp_{25}	$i_4 + nm_2 + nm_3 + a$
mp_{26}	$i_4 + nm_2 + nm_3 + d$
mp_{27}	$nm_1 + nm_2 + a$
mp_{28}	$nm_1 + nm_2 + d$
mp_{29}	$i_4 + d$
mp_{30}	$i_4 + a$